Linear and Nonlinear Controller Design for Robust Automatic Steering

Jürgen Ackermann, Jürgen Guldner, Wolfgang Sienel, Reinhold Steinhauser, and Vadim I. Utkin

Abstract— **For an automatic steering problem of a city bus the reference maneuvers and specifications are introduced. The robustness problem arises from large variations in velocity, mass, and road-tire contact. Two controller structures, both with feedback of the lateral displacement and the yaw rate, are introduced: a linear controller and a nonlinear controller. The controller parameters are first hand-tuned and then refined by performance vector optimization. Both controllers meet all specifications. Their relative merits are analyzed in simulations for four typical driving maneuvers.**

I. Introduction

AUTOMATIC steering of vehicles is of practical interest, e.g., for transport vehicles in factories and ship docks, for buses on separate, narrow (i.e., cheap) lanes, and in the future as part of an integrated system of automated highway traffic. The primary task of automatic steering is to track a reference path, where the displacement from the guideline is measured by a displacement sensor. The reference may consist of the magnetic field of an electrically supplied wire or permanent magnets in the road. The sensor is mounted in the center of the front end of the vehicle. The controller output acts on the front steering angle.

The design of an automatic steering system is a robustness problem in view of large variations in velocity and mass of the vehicle and contact between tire and road surface. In the present study, model data and specifications for a city bus O 305 are taken from the IFAC benchmark example [1]. A comparison will be made between linear and nonlinear controller concepts.

For linear control it was investigated in an earlier study [2], how the tracking accuracy is improved by additional feedback of the yaw rate which can be measured by a gyro. Thereby, the automatic steering problem becomes much less dependent on the uncertain operating conditions velocity, mass, and road-tire contact. The study showed a significant reduction in the displacement from the guideline for all maneuvers and operating conditions. In the present study the design method used in [2], the *Parameter Space Approach* is further exploited to explore extreme design directions. The resulting robust linear controller with *fixed* gains achieves good performance for a wide range of uncertainty in the operating conditions.

In the second part of this paper, a nonlinear controller structure is designed in an effort to further improve the performance of the automatic steering system. The nonlinear controller is based on *Sliding Mode Control* and includes dynamic adaptation to changing operating conditions via an estimator-like observer. The control design procedure is presented in a step-by-step manner. The advantages and drawbacks of the two approaches are contrasted in simulation studies.

Finally, controller parameters of both the linear and nonlinear controller are tuned automatically by optimizing a vector performance index such that the tracking performance for typical maneuvers is improved.

Manuscript received October 29, 1993; revised October 13, 1994. Recommended by Associate Guest Editor, U. Kiencke.

J. Ackermann, J. Guldner, W. Sienel, and R. Steinhauser are with the DLR, German Aerospace Research Establishment, Institute for Robotics and System Dynamics, Oberpfaffenhofen, D-82230 Wessling, Germany.

V. I. Utkin is with the Department of Electrical Engineering, The Ohio State University, Columbus, OH 43210–1107 USA.

IEEE Log Number 9408626.

II. Dynamic Model and Problem Statement

A. Model for Vehicle Dynamics

The classical single-track model is used to model the steering dynamics. It is obtained by lumping the two front wheels into one wheel in the centerline of the vehicle, the same is done with the two rear wheels, see Fig. 1.

In Fig. 1 the variables denote the following quantities: δ_f: steering angle; $\vec{v}$: velocity vector at the CG, its magnitude is $v>0$; β: sideslip angle between vehicle center line and $\vec{v}$; r: yaw rate; f_f (f_r): lateral forces generated by the front (rear) tire, acting on the chassis; f_w: wind forces acting on the aerodynamical center of the side surface; ℓ_w: distance between CG and aerodynamical center of the side surface; $\Delta\psi$: angle between centerline of vehicle and tangent to the guideline.

Together with the dynamics of the reference path and an actuator with integrating characteristics the vehicle dynamics is described by the fifth order model

$$\begin{bmatrix} \dot{\beta} \\ \dot{r} \\ \Delta\dot{\psi} \\ \dot{y} \\ \dot{\delta}_f \end{bmatrix} = \begin{bmatrix} a_{11} & a_{12} & 0 & 0 & b_{11} \\ a_{21} & a_{22} & 0 & 0 & b_{21} \\ 0 & 1 & 0 & 0 & 0 \\ v & \ell_s & v & 0 & 0 \\ 0 & 0 & 0 & 0 & 0 \end{bmatrix} \begin{bmatrix} \beta \\ r \\ \Delta\psi \\ y \\ \delta_f \end{bmatrix} + \begin{bmatrix} 0 & 0 & d_{11} \\ 0 & 0 & d_{21} \\ 0 & -v & 0 \\ 0 & 0 & 0 \\ 1 & 0 & 0 \end{bmatrix} \begin{bmatrix} u_f \\ \rho_{ref} \\ f_w \end{bmatrix} \quad (1)$$

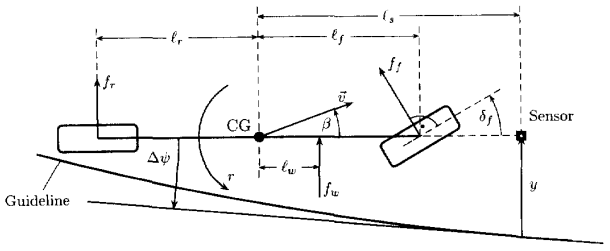

Fig. 1. Single-track model for car steering.

where

$$a_{11} = -(c_r + c_f)/\tilde{m}v \qquad b_{11} = c_f/\tilde{m}v$$
$$a_{12} = -1 + (c_r\ell_r - c_f\ell_f)/\tilde{m}v^2 \qquad b_{21} = c_f\ell_f/\tilde{J}$$
$$a_{21} = (c_r\ell_r - c_f\ell_f)/\tilde{J} \qquad d_{11} = 1/mv$$
$$a_{22} = -(c_r\ell_r^2 + c_f\ell_f^2)/\tilde{J}v \qquad d_{21} = \ell_w/J.$$

The cornering stiffnesses are written as a product μc_f for the front axle and μc_r for the rear axle, where μ is a common road adhesion factor with $\mu = 1$ for dry road and $\mu = 0.5$ for wet road. The vehicle mass m is normalized by μ, i.e., $\tilde{m} = m/\mu$ is a "virtual mass." Similarly, the moment of inertia J is normalized as $\tilde{J} = J/\mu$.

The curvature $\rho_{ref} = 1/R_{ref}$ of the guideline appears as a reference input to the system. It is assumed that the reference path consists of circular arcs, i.e., the transition to a new curvature corresponds to a step input in ρ_{ref}.

The data for the city bus O 305 are $\ell_f = 3.67\,\mathrm{m}$, $\ell_r = 1.93\,\mathrm{m}$, $\ell_s = 6.12\,\mathrm{m}$, $\ell_w = 0.565\,\mathrm{m}$, $c_f = 198000\,\mathrm{N/rad}$, $c_r = 470000\,\mathrm{N/rad}$, $v \in [1; 20]\,\mathrm{ms}^{-1}$, $m \in [9950; 16000]\,\mathrm{kg}$, $\mu \in [0.5; 1]$ and $J = i^2 m$, $i^2 = 10.85\,\mathrm{m}^2$. The parameter i is called "inertial radius." Sensors are available for the lateral deviation y and for the yaw rate r.

B. Design Specifications and Driving Maneuvers

The design specifications are taken from the IFAC benchmark example [1]. They are primarily given in terms of maximal displacement from the guideline and maximal steering angle and steering angle rate. In detail they are:

- The steering angle is limited to $|\delta_f| \leq 40$ deg.
- The steering angle rate is limited to $|\dot{\delta}_f| \leq 23$ deg s^{-1}.
- The displacement from the guideline must not exceed 0.15 m in transient state and 0.02 m in steady state.
- The lateral acceleration must not exceed 2 ms^{-2} for passengers comfort. The ultimate limit is 4 ms^{-2} for tip-over.
- The natural frequency of the lateral motion must not exceed 1.2 Hz.

The maximal displacement of 0.15 m is due to safety reasons, e.g., if the bus enters a bus stop bay where passengers are waiting to enter the bus.

The reference maneuvers considered for the simulations are:

- Transition from a straight line into a circle. The curve radius is $R_{ref} = 400$ m.
- Transition from manual to automatic operation. The bus is assumed to drive in a distance of $y = 0.15$ m parallel to the guideline when the control is activated. A fast transient is desired.
- Side wind forces. A gust of wind attacks the bus from the lateral direction. It is assumed that the wind velocity increases with $v_w = (1 - e^{-t/T})\,20\,\mathrm{m/s}, T = 0.5$ s.
- Entering into a narrow bus stop bay. The reference input ρ_{ref} is shown in Fig. 2. The admissable velocity should be 2.5 mg^{-1} or higher.

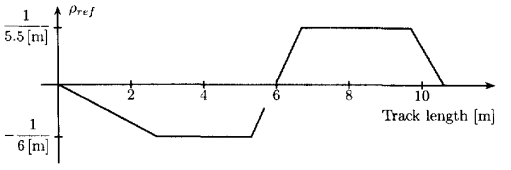

Fig. 2. Reference input ρ_{ref} for entering a bus stop bay.

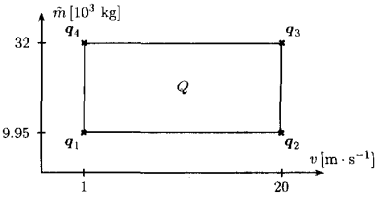

Fig. 3. Operating domain Q of the city bus.

All simulations are performed with the linear vehicle model (1) taking into account the actuator saturations $|\dot{\delta}_f| \leq 23\,\mathrm{deg\,s}^{-1}$ and $|\delta_f| \leq 40$ deg.

III. Linear Controller Design

The design of a robust automatic steering system for vehicles with fixed compensator transfer function is a challenging task due to the large uncertainty in velocity v and virtual mass $\tilde{m} = m/\mu$. The domain Q of possible operating conditions for the city bus O 305 is given in Fig. 3 where a road adhesion factor $\mu \in [0.5; 1]$ is assumed, such that $\tilde{m} \in [9950; 32000]$ kg. Since the bus is not controllable for $v = 0$, a minimum velocity of $v^- = 1\,\mathrm{ms}^{-1}$ is assumed. The extremal vertex plants are denoted by $\boldsymbol{q}_1$ to $\boldsymbol{q}_4$, where $\boldsymbol{q} := [v\,\tilde{m}]^T$.

In earlier design studies, e.g., [2], it turned out that a hard design conflict exists between the 23 deg s^{-1} constraint on the steering angle rate when entering a narrow bus stop bay and good track following at all speeds. In [2] it was shown that additional feedback of the yaw rate leads to a significant reduction of the deviation from the guideline in nearly all driving maneuvers compared to earlier controller designs which used solely feedback of the deviation y. The present design study is based on the approach in [2] and will investigate extreme design directions.

A. Selecting a Controller Structure

In [2], feedback of the yaw rate with

$$\dot{\delta}_f = u_f - k_r \cdot r \tag{2}$$

was proposed. Fig. 4 shows the root locus of the transfer function $r(s)/u_f(s)$ with feedback (2) in dependency of the

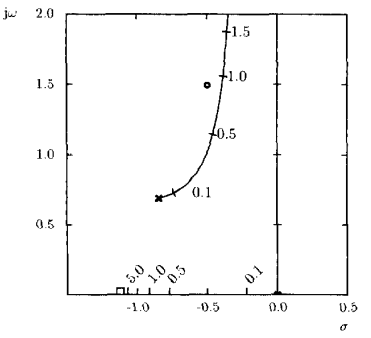

Fig. 4. Root locus of the transfer function from u_f to r for increasing gain k_r. The zeros of the transfer function $y(s)/u_f(s)$ are marked with circles, the zero of $r(s)/u_f(s)$ with a square.

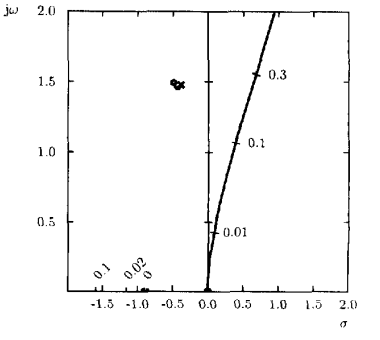

Fig. 5. Root locus of the transfer function from u_f to y with yaw rate feedback $k_r = 0.89$.

gain k_r, where the operating point with maximal virtual mass and maximal velocity was selected, which turned out to be the most critical operating condition in an eigenvalue analysis [3]. The feedback law (2) shifts the poles of the transfer function $r(s)/u_f(s)$, which are also poles of the transfer function $y(s)/u_f(s)$. There occurs an almost cancellation of a pole/zero-pair in the transfer function from u_f to y for $k_r \approx 0.89$. This reduces the influence of the complex pole pair on the time responses. The tracking controller will be designed with the fixed feedback gain $k_r = 0.89$.

The vehicle with yaw rate feedback is now considered for design of an outer loop with feedback of y to u_f via a compensator. A compensator structure for feedback of the sensor displacement from the guideline can be determined by root locus considerations. In Fig. 5 the root locus with proportional feedback of the deviation y to u_f is shown. By the control law (2) one of the three poles at $s = 0$ has been shifted to $s = -0.8934$. From the remaining two poles at $s = 0$, two root locus branches start under ± 90 deg and turn into the right-half plane to converge to asymptotes under an angle of ± 60 deg. Obviously, two zeros are necessary in the left-half plane to attract these two branches. These considerations suggest a compensator transfer function

$$\omega_c^2 \frac{k_{DD}s^2 + k_D s + k_P}{s^2 + 2D\omega_c s + \omega_c^2}$$

where inside the bandwidth ω_c we have a proportional part k_P, a differential part k_D, and a double differential part k_{DD}. The above controller structure, however, leads to an undesired stationary error in curve riding. To avoid this an integrating term k_I/s in the numerator of the controller transfer function has to be added. The PIDD^2 controller transfer function then becomes

$$f_c(s) = \omega_c^3 \frac{k_{DD}s^2 + k_D s + k_P + k_I/s}{(s^2 + 2D\omega_c s + \omega_c^2)(s + \omega_c)} \tag{3}$$

where a third real compensator pole with the same bandwidth ω_c was chosen. The final controller structure with yaw rate and displacement feedback is shown in Fig. 6.

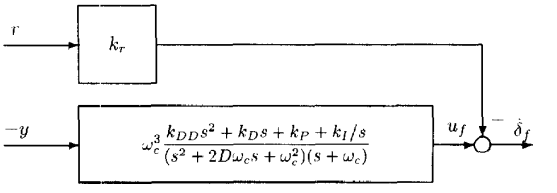

Fig. 6. Controller structure.

TABLE I
POLES AND ZEROS OF THE TRANSFER FUNCTION $y(s)/u_f(s)$ WITH YAW RATE FEEDBACK $k_r = 0.89$ FOR THE CITY BUS O 305. THERE IS AN ADDITIONAL DOUBLE POLE AT THE ORIGIN

Operating condition	Poles	Zeros
1	-0.1595	-0.1245
	-39.66	
	-68.20	-63.78
2	$-1.209 \pm j2.402$	$-1.598 \pm j2.321$
	-2.984	
3	-0.8934	$-0.4968 \pm j1.491$
	$-0.3930 \pm j1.476$	
4	-0.1608	-0.1250
	-12.25	
	-21.17	-19.75

B. The Parameter Space Approach

To illustrate the different system dynamics for varying operating conditions, the poles and zeros of the transfer function $y(s)/u_f(s)$ of the bus O 305 with yaw rate feedback ($k_r = 0.89$) are calculated in Table I for the four extremal plants, see Fig. 3. For low velocities (operating conditions 1 and 4) a real pole is close to the origin, for high velocities (operating conditions 2 and 3) a weakly damped complex pole pair is critical. In all four cases the influence of these critical poles on the time response of the system is decreased by zeros in their neighborhood which was intended by proportional feedback of the yaw rate.

Conventional methods for controller design like pole placement yield a unique controller for each plant, i.e., no further robustness criteria can be incorporated in the design step. The parameter space approach, on the other hand, can be used to determine a set of coefficients for a given controller structure which simultaneously stabilize a finite number of plants.

More generally speaking, the parameter space approach allows to determine the set of parameters $\mathcal{H}$, for which the characteristic polynomial $p(s, \boldsymbol{h}), \boldsymbol{h} \in \mathcal{H}$, is stable. The parameter vector $\boldsymbol{h}$ may consist of uncertain plant parameters $\boldsymbol{q}$, like v and $\tilde{m}$ in the present example. Then, the parameter space approach can be utilized for stability analysis [4]. The plant is robustly stable if the operating domain is entirely contained in the set of stable parameters: $Q \subset Q_{\text{stable}} := \mathcal{H}$. In the case of controller parameters $\boldsymbol{k}$, the set $\mathcal{K} := \mathcal{H}$ of stabilizing controller parameters can be determined [3], i.e., each controller from the set $\mathcal{K}$ will stabilize the given plant.

The procedure for determining the stability regions in $\boldsymbol{h}$-space for Hurwitz-stability is as follows: First, the real and imaginary parts of the characteristic polynomial are determined for $s = j\omega$

$$p(j\omega, \boldsymbol{h}) = \operatorname{Re} p(\omega, \boldsymbol{h}) + j \operatorname{Im} p(\omega, \boldsymbol{h}).$$

The frequency ω is gridded in the interval $\omega \in [0; \infty)$ and for each grid point $\omega = \omega^*$ the simultaneous solution of the two equations

$$\begin{aligned} \operatorname{Re} p(\omega^*, \boldsymbol{h}) &= 0 \\ \operatorname{Im} p(\omega^*, \boldsymbol{h}) &= 0 \end{aligned} \tag{4}$$

is determined. An explicit solution is only possible for a two-dimensional $\boldsymbol{h}$-space. Therefore, a two-dimensional cross section in $\boldsymbol{h}$-space has to be fixed before solving (4), if dim $\boldsymbol{h} > 2$. A simple choice of such a cross section is fixing all but two parameters, say $h_3, h_4, \cdots$. Then, (4) depends only on h_1 and h_2 and the resulting solutions can be visualized in the (h_1, h_2)-plane.

For the problem of automatic track guiding, Hurwitz-stability is not sufficient. A hyperbola in the s-plane is selected to guarantee settling time and damping values for the worst case. The eigenvalues of the closed-loop system should lie in the region Γ on the left-hand side of the boundary

$$\partial\Gamma = \left\{ s = \sigma + j\omega \,\middle|\, \left(\frac{\sigma}{\sigma_0}\right)^2 - \left(\frac{\omega}{\omega_0}\right)^2 = 1,\ \sigma \le -\sigma_0 \right\}. \tag{5}$$

The parameters σ_0 and ω_0 are chosen according to the basic rule of robust control [3]: Leave a slow system slow and a fast system fast. Applied to the present problem this means not to shift the real pole which lies close to the origin for low velocities too far into the left-half plane. On the other hand it is not desired to have real poles close to the origin at high speeds in order to avoid a sluggish response. For this reason two different values for σ_0 are chosen in dependency of the velocity: $\sigma_0 = 0.12$ for low velocities and $\sigma_0 = 0.35$ for high velocities. The parameter ω_0 which determines the damping of the hyperbola for $\sigma \mapsto -\infty$ for fixed σ_0 is set such that $\omega_0/\sigma_0 = 5$ which corresponds to a damping of 0.196. The eigenvalues of Table I are all located in the admissible region Γ. The main task of the control is to shift the two eigenvalues at the origin into the region Γ. If all eigenvalues of the closed loop system are located in the region Γ then the plant is called Γ-stable.

For each of the four extremal plants (see Fig. 3) with controller (3), the boundary $\partial\Gamma$ of the region Γ in the complex eigenvalue plane will be mapped into controller coefficient space resulting in four Γ-stabilizing regions. Their intersection is the set of simultaneous Γ-stabilizers for the four extremal plants [3].

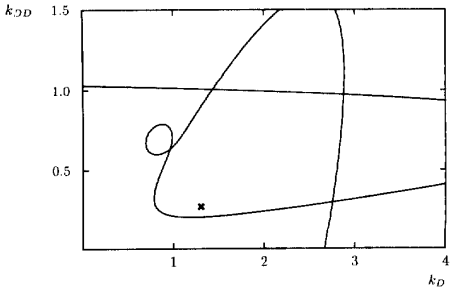

Fig. 7. Set of Γ-stabilizing controllers for operating point $\boldsymbol{q}_3$.

The Γ-stability boundaries will be displayed in the (k_D, k_{DD})-plane. These two parameters are involved in determining the location of the zero pair that should pull the right-half plane branches of the root locus of Fig. 5 into the left-half plane. Initial values for the controller parameters are taken from [2]. The compensator transfer function obtained there was

$$f_{c1}(s) = 40^3 \frac{0.27s^2 + 1.3s + 1.9 + 0.75/s}{(s^2 + 2 \cdot 0.6 \cdot 40s + 40^2)(s + 40)}. \tag{6}$$

It robustly stabilizes the given operating domain Q, but it does not meet all specifications.

With the fixed controller parameters $k_P = 1.9, k_I = 0.75, D = 0.6$, and $\omega_c = 40$ from (6), the closed-loop polynomial $p(s, k_D, k_{DD})$ depends only on k_D and k_{DD}. For $s = \sigma(\alpha) + j\omega(\alpha), \sigma = -\alpha$, where $\omega(\alpha)$ satisfies (5), real and imaginary part of the characteristic polynomial can be determined. The boundary parameter α is gridded in the interval $\alpha \in [\sigma_0; \infty)$ and for each grid point α^* the set of equations (4) is solved for k_D and k_{DD}.

As an example the Γ-stability boundaries for the operating point $\boldsymbol{q}_3$, i.e., $\sigma_0 = 0.35$, are shown in Fig. 7. The Γ-stability boundaries divide the parameter plane into a finite number of separated regions. By selecting one arbitrary point from each region, the set of Γ-stabilizing controllers is determined: If one point of a region turns out to be Γ-stable then the entire region is Γ-stable, and vice versa. The point (1.3, 0.27) marked with a cross is Γ-stable and, hence, all controller parameters from the entire region indicated by the cross Γ-stabilize the plant $\boldsymbol{q}_3$.

In this example, it was demonstrated how to determine the set of Γ-stabilizing controllers for one extremal plant. In the same manner the set of Γ-stabilizing controllers can be determined for the other extremal plants. If there exists an intersection of these Γ-stabilizing sets, then the controller parameters from this intersection simultaneously Γ-stabilize the considered plants. The four vertex plants $\boldsymbol{q}_1$ to $\boldsymbol{q}_4$ (see Fig. 3) are taken as representatives for the present controller design. Once a controller is determined, a stability analysis of the selected controller has to verify Γ-stability for the entire plant family [3].

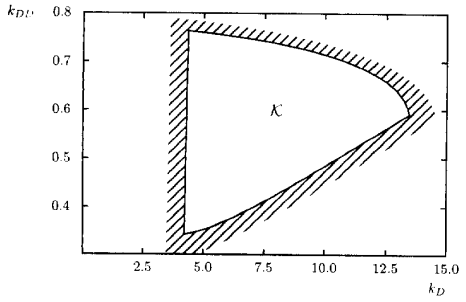

Fig. 8. Set of Γ-stabilizing controllers for $\omega_c = 100$, $D = 0.5$, $k_I = 3$, and $k_P = 10$.

C. Investigation of Extreme Design Directions

In view of actuator constraints and passenger comfort, i.e., small lateral accelerations and low natural frequency ω_n of the lateral motion, a controller with low gains and low bandwidth looks promising. On the other hand, low gain controllers lead to unsatisfactory path following. The controller (6) can be considered as a compromise solution which allows good track following at all speeds and has a sufficiently small bandwidth ω_c. This controller will be used as comparison for further controller designs.

Simulation results for maximal virtual mass for the controller (6), taking into account the actuator constraints, are shown in Figs. 9–10 with dashed lines. The maximal speed for entering a narrow bus stop bay with maximal virtual mass is 1.3 ms^{-1}, for higher velocities the deviation from the guideline exceeds 0.15 m. All other maneuvers were simulated for maximal speed $v = 20\,\mathrm{m\,s}^{-1}$.

It is desired to enter the bus stop bay at higher speeds, and the controller has to be redesigned. The deviation from the guideline will certainly get smaller with increasing controller gains and controller bandwidth. An interesting question which arises at this point is: Find controller parameters such that the admissible speed for entering the bus stop bay gets as large as possible.

Taking the controller parameters from (6) as initial values a set of Γ-stabilizing controller parameters with larger bandwidth can be found by the parameter space approach. The (k_D, k_{DD})-plane is used as cross section in parameter space to visualize the set of Γ-stabilizing controllers. It is known from controller (6) that it Γ-stabilizes the entire plant, i.e., a set of simultaneously Γ-stabilizing controller parameters for the four vertex plants can be determined in the (k_D, k_{DD})-plane.

By small modification of the remaining parameters k_P, k_I, and D, one can find directions in this three-dimensional subspace for which the set of Γ-stabilizing controllers grows or shrinks. Once the largest set is determined, the controller parameter ω_c is increased stepwise and in each step the free parameters k_P, D, and k_I, are tuned such that the set of simultaneously Γ-stabilizing controllers gets as large as possible.

After each iteration step, some controllers from the simultaneously Γ-stabilizing set are tested in simulations and the maximal velocity for entering the bay is determined. During the iterations one recognizes that no significant rise in the maximal velocity for entering the bus stop bay occurs if the bandwidth is increased beyond $\omega_c = 100$. The set $\mathcal{K}$ of simultaneously Γ-stabilizing controllers for the four vertex plants for $\omega_c = 100, D = 0.5, k_P = 10$, and $k_I = 3$, is displayed in Fig. 8.

The simultaneously Γ-stabilizing set $\mathcal{K}$ in Fig. 8 allows a wide range in the parameters k_D and k_{DD}. Several controllers from this set are tested in simulations and it turns out that the control performance is best for larger k_D. Finally, the controller

$$f_{c2}(s) = 100^3 \frac{0.6s^2 + 13s + 10 + 3/s}{(s^2 + 100s + 100^2)(s + 100)} \tag{7}$$

is selected. In an analysis of the closed loop Γ-stability can be proved for this controller, see [4], [3] for details about utilizing the parameter space approach for robustness analysis.

With the controller (7) the maximum speed for entering the bus stop bay is 2.63 $\mathrm{m\,s}^{-1}$. Simulation results for the controller are displayed with solid lines in Figs. 9 and 10. The maneuver for entering the bay was simulated for $v = 2.5\,\mathrm{m\,s}^{-1}$, the other maneuvers at maximal speed $v = 20\,\mathrm{m\,s}^{-1}$. Compared to the compensator (6) the deviations for crosswind and cornering are significantly reduced. It is surprising, however, that the deviation for switching from manual to automatic steering converges slower to the guideline than for controller (6). Due to the higher gains the controller makes use of the maximal steering angle rate of 23 deg s^{-1} as shown in Fig. 10. The lateral accelerations at the sensor position are larger compared to the simulation results of controller (7), but they are still in the admissible range.

With the help of the parameter space approach it was possible to find a set of simultaneously Γ-stabilizing controllers for the four vertex plants for a given bandwidth ω_c. A compromise solution for ω_c has to be determined weighing between slow responses and low velocity for entering the bus stop bay at low controller bandwidth (6) and larger lateral acceleration and higher natural frequency of the lateral motion at high controller bandwidth (7). The lateral acceleration in Fig. 10 shows that the "tight" control by (7) requires faster motions at higher frequencies than the "soft" control by (6).

The hand-tuning procedure provides good initial values for fine-tuning by optimization in Section V.

IV. Design of a Nonlinear Controller

In this section, we describe a different approach to design a robust controller for automatic steering of the city bus O 305. The control methodology is based on *sliding mode control* theory and robust state observation. A suitable cascaded controller structure is developed step-by-step, including a stability analysis. The nonlinear control design procedure, in contrast to linear controller design methods, accounts for actuator constraints and provides adaptation to changing operating conditions via state and uncertainty observation. The control parameters are first hand-tuned using simulations and then optimized with the control design package ANDECS, developed at DLR.

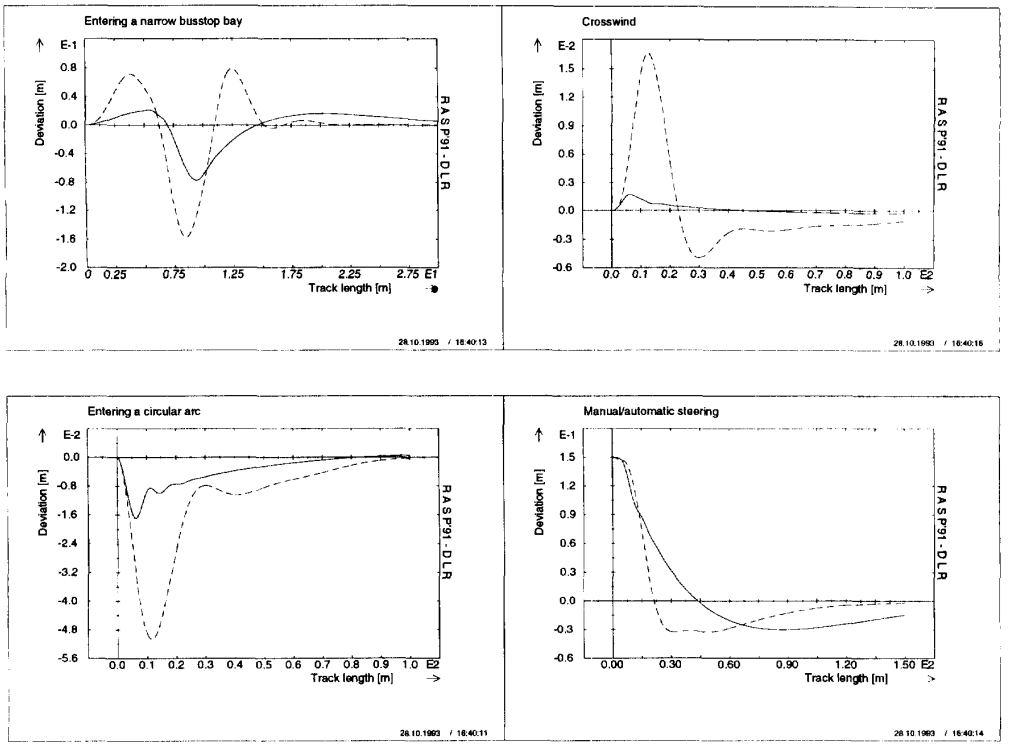

Fig. 9. Simulation results: Deviation from the guideline (dashed: controller (6), solid: controller (7)).

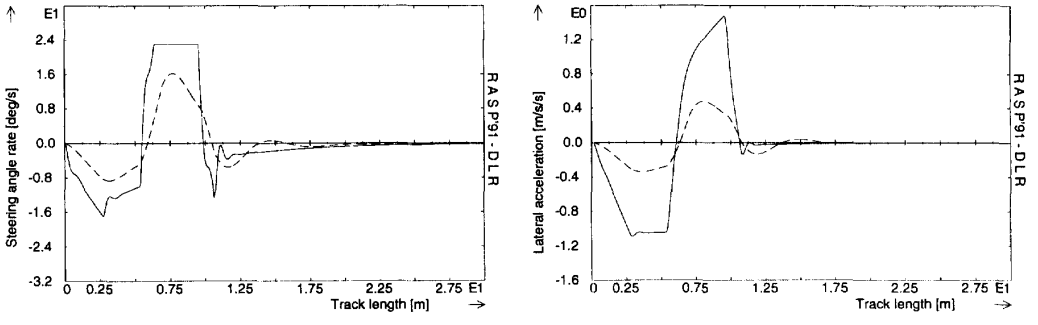

Fig. 10. Simulation results: Steering angle rate (dashed: controller (6), solid: controller (7)).

A. Brief Introduction to Sliding Mode Control

Sliding mode control is known to enable implementation of (theoretically) infinitely high gains with bounded control actions, resulting in robustness with respect to plant uncertainty and external disturbances. The basic idea is to restrict the state space trajectories of the dynamic system to a manifold called "sliding manifold," denoted by $S(x) = 0$. This is achieved by directing the system trajectories towards this manifold "from both sides" (see Fig. 11) using two different controls u^+ and u^-. Consequently, the control is switched discontinuously each time the trajectory crosses the manifold $S(x) = 0$, resulting in a *variable structure* of the system equations. The main benefits of sliding mode control are its invariance properties and the ability to decouple high dimensional problems into subtasks of lower dimensionality. The interested reader is referred to [5] for a more detailed introduction to sliding mode and variable structure systems.

An inherent disadvantage of high gain feedback is its tendency to excite unmodeled dynamics, for example those of actuators. In particular, discontinuous switching of the control along the sliding manifold leads to the so-called "chattering problem," inhibiting direct implementation of sliding mode control. A well-studied, reliable remedy is the utilization of observers as a by-pass for the high-frequency component in the control signal. The introduction of an observer preserves the properties of sliding mode control, the system performance

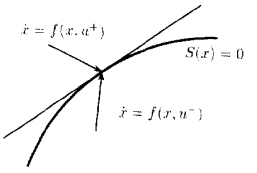

Fig. 11. State velocity vectors in the vicinity of the sliding manifold.

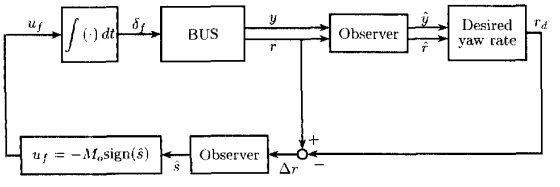

Fig. 12. Nonlinear controller structure with observer.

being close to the "ideal" case, but exhibiting no oscillatory behavior or chattering [6].

At first sight, the design of an observer, for example of Luenberger-type, requires knowledge of the plant parameters. However, assuming slowly time-varying uncertainties (in comparison to the observer dynamics), an observer-like compensator can be used to estimate the uncertainty-terms. The sensitivity to uncertain parameters may be decreased by high observer gains. However, a compromise is needed to prevent excitation of unmodeled dynamics. The estimation observer proved to be an efficient tool to provide the necessary adaptation to changes in operating conditions.

The proposed cascaded nonlinear control strategy requires only measurement of the displacement y from the guiding wire and of the vehicle yaw rate r, as the linear controller of Fig. 6. Due to the estimation properties of the observer, the nonlinear controller is robust with respect to the desired range of operating conditions.

B. Cascaded Nonlinear Control Design

To facilitate the analysis, control design is based on the output dynamics of the single track model (1)

$$\dot{y} = v(\beta + \Delta\psi) + l_s r. \tag{8}$$

The fundamental idea of cascaded nonlinear control design is to first determine a "feedback" law for the desired yaw rate r_d for (8) viewing the yaw rate r as a "fictitious" control input. In a second step, the actual control u_f is derived based on the dynamics of r to drive the error $\Delta r = r - r_d$ between the actual yaw rate and the desired yaw rate to zero. This decoupling of the design procedure is made possible by the availability of the yaw rate r measured by a gyroscope. The full cascaded nonlinear control algorithm is sketched in Fig. 12.

1) Step I: Desired Yaw Rate Controller: Following the lines of traditional feedback linearization, the desired yaw rate would be determined as

$$r_d = -\frac{1}{l_s}(v(\beta + \Delta\psi) + K y), \qquad K > 0 \tag{9}$$

where K determines the desired rate of decay of y. However, both the states β and $\Delta\psi$ and the velocity v are unknown.

In order to obtain an estimate of the term $q := v(\beta + \Delta\psi)$, dynamic estimation via an observer is utilized, assuming $\dot{q} \approx 0$. The observer equation is defined to be

$$\begin{aligned} \dot{\hat{y}} &= \hat{q} + \ell_s r + \ell_1 \overline{y}, \qquad \ell_1 > 0 \\ \dot{q} &= \ell_2 \overline{y}, \qquad \ell_2 > 0 \end{aligned} \tag{10}$$

where $\overline{y} = y - \hat{y}$ is the observation error for the lateral displacement.

The observation errors $\overline{y}$ and $\overline{q}$ can be made small even for $\dot{q} \neq 0$ by choosing ℓ_1 and ℓ_2 such that the observer dynamics are at least one order of magnitude faster than those of q. The observer (10) has the structure of a Kalman-filter and, thus, can be expected to exhibit advantageous filtering properties in the presence of measurement noise.

The estimates $\hat{y}$ and $\hat{q}$ are used for the desired yaw rate (9) to yield

$$r_d = -\frac{1}{\ell_s}(\hat{q} + K\hat{y}). \tag{11}$$

The entire closed-loop error system (still assuming $r = r_d$ and $\dot{q} \approx 0$) is given by

$$\begin{bmatrix} \dot{y} \\ \dot{\overline{y}} \\ \dot{\overline{q}} \end{bmatrix} = \begin{bmatrix} -K & K & 1 \\ 0 & -\ell_1 & 1 \\ 0 & -\ell_2 & 0 \end{bmatrix} \begin{bmatrix} y \\ \overline{y} \\ \overline{q} \end{bmatrix}. \tag{12}$$

Summarizing the first step of the control design procedure, we can state that good tracking of the guiding wire is provided if the yaw rate of the vehicle is equal (or close) to the desired yaw rate as defined in (11). Note that the calculation of r_d requires only measurement of the lateral displacement y from the reference trajectory and the vehicle yaw rate r. No knowledge of the system parameters except for ℓ_s is required.

2) Step II: Control of Steering Angle Rate: The second step in the design procedure concentrates on determining a suitable control command u_f to drive the error $\Delta r = r - r_d$ to zero. The proposed control algorithm is based on sliding mode theory. The sliding manifold is defined to be

$$S = c\Delta r + \Delta\dot{r} \tag{13}$$

where $c > 0$ is a constant gain determining the system behavior once the motion of (13) has been restricted to the manifold $S = 0$.

To suppress uncertainty due to unknown parameters and disturbance ρ_{ref}, let

$$u_f = -M_u \text{sign}(S) \tag{14}$$

where $M_u > 0$ is the available steering angle rate.

In the first step of the design procedure in Section IV-B1 it was shown that good tracking of the guiding wire is

achieved under the assumption that the yaw rate r of the vehicle is equal to r_d of (11). The complete system is expected to exhibit satisfactory performance if the error Δr is small. The stability of Δr is analyzed using the positive definite *Lyapunov-function* candidate

$$V = \frac{1}{2}S^2 \tag{15}$$

for S in (13). Differentiating (15) along the system trajectories under the control (14) yields

$$\begin{aligned}\dot{V} &= S\dot{S} \\ &= S(h(\beta, r, \Delta\psi, y, \delta_f, \rho_{ref}, \hat{y}, \hat{q}) + b_{21}u_f) \\ &\leq -M_u b_{21}|S| + |h(\cdot)|\,|S|\end{aligned} \tag{16}$$

where $h(\cdot)$ is unknown, but upper bounded, and independent of the control u_f.

Since $b_{21} > 0$ in (1), there exists a finite M_u such that

$$M_u > \max\left(\frac{|h(\cdot)|}{b_{21}}\right) \tag{17}$$

for all operating conditions. Hence, (16) implies together with V in (15)

$$\dot{V} \leq -\xi V^{1/2} \tag{18}$$

for some positive scalar ξ. It was established in [5] that V, and consequently S, converge to zero after finite time. Consequently, the yaw rate error Δr tends to zero at a rate specified by parameter c in (13). Boundedness of $|h(\cdot)|$ is ensured by virtue of bounded states β, r, and δ_f, bounded parameters a_{ij} and $b_{i1}(i, j = 1, 2)$ in (1), and bounded continuous desired yaw rate r_d as defined in (11).

Control law (14) depends on Δr and $\Delta\dot{r}$, in other words on r, $\dot{r}$, r_d, and $\dot{r}_d$. While $\dot{r}_d$ could be calculated from (11) and (10), $\dot{r}$ is unknown. Since the dynamics of r are relatively slow due to the inertia of the bus, the first idea is to obtain $\Delta\dot{r}$ by a differentiating filter. However, the dynamics of a differentiator prevent *ideal* sliding mode to occur [5] and may lead to chattering and, thus, to unsatisfactory performance. A remedy is to use an observer to estimate the time-derivative of Δr as will be illustrated in the next section.

3) Step III: Design of Robust Observer: For convenience, denote $z_1 = \Delta r$ and $z_2 = \Delta\dot{r}$. The goal is to design an observer for the system

$$\begin{aligned}\dot{z}_1 &= z_2 \\ \dot{z}_2 &= f(\beta, r, \delta_f, \rho_{ref}, u_f)\end{aligned} \tag{19}$$

where $f(\cdot)$ is bounded since all states, all parameters, and control u_f are bounded.

We define an observer as follows

$$\begin{aligned}\dot{\hat{z}}_1 &= \hat{z}_2 + M_1\overline{z}_1 \\ \dot{\hat{z}}_2 &= \hat{f}(\cdot) + M_1M_2\overline{z}_1\end{aligned} \tag{20}$$

with $M_1 \gg M_2 > 0, \overline{z}_1 = z_1 - \hat{z}_1 = \Delta r - \hat{\Delta r}$, and $\hat{f}(\cdot)$ being an estimate of $f(\cdot)$. In general, the estimate $\hat{f}(\cdot)$ depends on the modeling effort and on the computational complexity allowable in the observer realization. In the particular case studied in this paper, the accuracy of $\hat{f}(\cdot)$ is limited by the parametric uncertainty in the model and the absence of state measurements except for r_d, $\dot{r}_d$, r, y, and u_f.

Subtracting (20) from (19) leads to the observer error-system

$$\dot{\overline{z}}_1 = \overline{z}_2 - M_1\overline{z}_1 \tag{21}$$

$$\dot{\overline{z}}_2 = \overline{f}(\cdot) - M_2M_1\overline{z}_1 \tag{22}$$

where $\overline{f}(\cdot) = f(\cdot) - \hat{f}(\cdot)$ is an estimation error.

It has been shown in [5] that $\hat{z}_1 \approx z_1 = \Delta r$ and $\hat{z}_2 \approx z_2 = \Delta\dot{r}$. This result follows from the *equivalent control method* [5] and the equivalency of high-gain systems and variable structure systems [7]. Explicitly, $\overline{z}_1 \to 0$ in (21) for large M_1. According to [5], [7], the resulting behavior can be analyzed by formally setting $\dot{\overline{z}}_1 = 0$. Thus, $\overline{z}_2 = M_1\overline{z}_1$, which is substituted into (22) to obtain $\dot{\overline{z}}_2 = \overline{f}(\cdot) - M_2\overline{z}_2$, and consequently $\overline{z}_2 \to 0$ for large M_2. Condition $M_1 \gg M_2$ establishes motion rate hierarchy and sequential convergence to zero of the observation errors in (21) and (22).

The estimates $\hat{z}_1$ and $\hat{z}_2$ replace the exact term Δr and the differentiated term $\Delta\dot{r}$ in (13), respectively, and ideal sliding mode occurs in the observed variable $\hat{S} = c\hat{z}_1 + \hat{z}_2$. The behavior of the true system (19) will differ from the observer system (20) by the order of the observation errors (21) and (22), which can be arbitrarily adjusted by sufficiently high gains M_1 and M_2. Little knowledge of plant parameters is required, in other words, the estimate $\hat{f}(\cdot)$ can be composed of a few simple terms. For finite gains $M_i, i = 1, 2$, it can be shown that the resulting observation error is of $\mathcal{O}(1/M_i)$ order. Since observer (20) has a Kalman filter structure similar to (10), filtering of measurement noise can be achieved for appropriate finite M_i. This leads to a design conflict between the need to suppress the uncertainty in $\overline{f}(\cdot)$ with *high* gains and the desire to enhance noise filtering properties with *low* gains. A possible remedy is to use a third order observer instead of (20) with $z_3 = f(\cdot)$, assuming $\dot{f}(\cdot) \approx 0$, see also [8], [9].

Summarizing the controller design, we can conclude that the interconnected control system (11) and (14), in combination with the observer (20) exhibits good performance for sufficient amplitude M_u of control. Practical considerations on the choice of control parameters in the face of actuator constraints will be discussed in the following section.

The controller is *independent* of all plant parameters except for the length l_s and it only requires measurement of the yaw rate r and the lateral displacement from the guiding wire, y. Due to the estimation properties of the sliding mode observer, the control algorithm is robust with respect to all "reasonable" operating conditions. Fig. 12 illustrates the complete nonlinear control algorithm.

4) Hierarchy of Gains for Nonlinear Controller: The plant as described in (1) is a dynamic system of fifth order. It is important to maintain the resulting hierarchy of time scales when determining the gains of the cascaded control loops: The outermost loop in y has to be kept "slower" than the middle loop in β, r, and $\Delta\psi$, whereas the innermost loop in δ_f can be made arbitrarily fast, being constrained only by limitations

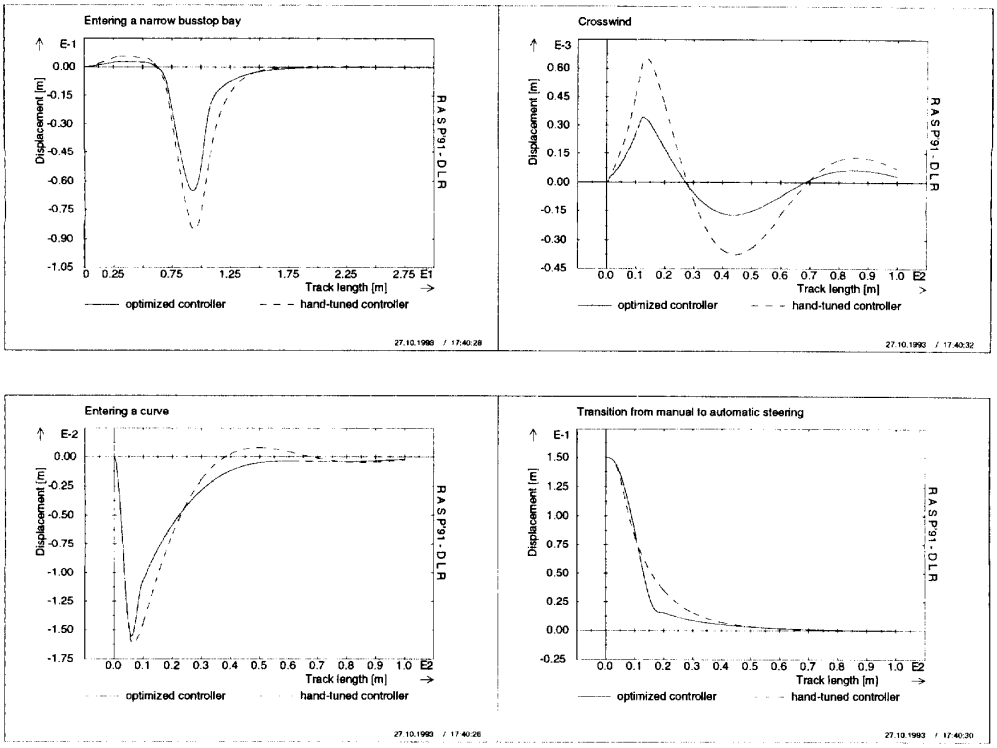

Fig. 13. Lateral displacement for nonlinear controller.

TABLE II
HAND-TUNED PARAMETERS FOR NONLINEAR CONTROLLER

Desired Yaw Rate				Sliding Mode Controller		
λ	ϵ	ℓ_1	ℓ_2	c	M_1	M_2
13	2	100	25	0.6	400	100

of the control amplitude. The dynamic observers, on the other hand, should have time constants about one order of magnitude higher than the respective closed loop.

The derivation in the previous sections neglected the limitations of the actuator when imposing condition (17). In reality, $M_a \leq 23$ deg s^{-1}, as outlined in the specifications. The constraints require to determine the control parameters in inverse order, starting from the outermost loop and then following the hierarchy described above.

To improve passenger comfort, it proved to be advantageous to replace the linear term $K\hat{y}$ in (11) by a saturation function:

$$r_d = -\frac{1}{\ell_s}\left(\hat{q} + \lambda \frac{\hat{y}}{\sqrt{\hat{y}^2 + \epsilon}}\right), \quad \lambda > 0, \quad \epsilon > 0. \tag{23}$$

The slope in the origin, λ/ϵ, should be chosen appropriately in order to yield the desired system behavior. The small-signal behavior remains unchanged for $K = \lambda/\epsilon$, but the amplitude of the feedback term is limited by λ, resulting in a smoother transition in the face of an initial error in y. The price for improving the ride quality is a slightly slower convergence, especially for large deviations y.

In contrast to linear control systems, a high controller bandwidth actually tending to infinity for ideal switching in (14), *does not* lead to a high closed loop bandwidth. In fact, it was shown in [5] that "in sliding mode" (e.g., when $S \equiv 0$), the average of control is close to the *equivalent control* obtained by setting $\dot{S} = 0$. Consequently, the closed loop behavior is solely determined by the controller gains λ/ϵ and c and the observer gains l_1, l_2, M_1, and M_2. This enables analytical examination of the closed loop eigenvalues of the automatic steering system under the discontinuous control (14).

Discretisation of a controller structure similar to the above design can be found in [9] for automatic car steering.

C. Numerical Studies

Simulations were used to determine "hand-tuned" parameters for the nonlinear control algorithm introduced in the previous sections. The linearized model (1) was used for all studies. Studies for automatic car steering showed no significant deterioration when using a full-scale nonlinear model [8]. The hand-tuned controller (see Table II) served as a starting point for optimization with the optimization module MOPS provided within the control design package ANDECS developed at DLR. The optimization procedure for both the linear and the nonlinear controller is summarized in Section V.

Since the simulations for the nonlinear controller are more valuable after the optimization procedure, the results are

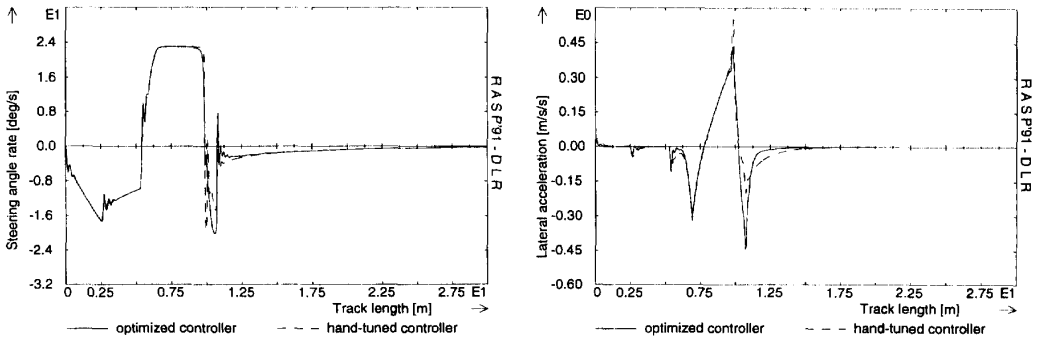

Fig. 14. Steering angle rate and lateral acceleration for the nonlinear controllers for entering a narrow bus stop bay.

displayed in Section V. For the simulations, the discontinuous switching function in the sliding mode controller (14) was substituted by a continuous approximation

$$u_f = -M_u \frac{S}{\sqrt{S^2 + 0.0001}}. \tag{24}$$

This results in a continuous control u_f.

V. Tuning of Controller Parameters by Optimizing a Vector Performance Index

Two different controller structures have been developed for automatic steering: The linear controller (7) and the nonlinear controller (23), (13), (14). The two controllers found so far by hand-tuning can be judged by Fig. 9 for the linear controller and by the dashed graphs of Fig. 13 for the nonlinear controller. Both controllers guarantee robust stability for the data of a city bus O 305 and show well behaved steering performance. Nevertheless, the controllers exhibit a slow transition from manual to automatic operation.

The question arises whether controller coefficients can be found which result in a faster transition behavior without deterioration of the already gained control performance in the other maneuvers. For investigating such a specified design direction, manual tuning of controller coefficients is not practical. Rather, a design procedure is required which allows direct inclusion of the respective design specifications and which can be steered into the desired design direction.

An efficient procedure is controller design based on optimizing a vector performance index [10], [3]. This approach allows direct inclusion of specific requirements into the design, for instance for the maximal displacement. The design requirements are formulated mathematically by criteria $c_i = c_i(\boldsymbol{k})$ with values depending on the controller coefficients $\boldsymbol{k}$. For each criterion c_i a design parameter d_i is chosen in a systematic manner that allows to steer the design in a desired direction. The scalar function $\gamma(\boldsymbol{k}) = \max_i c_i(\boldsymbol{k})/d_i$ is minimized over $\boldsymbol{k}$ resulting in a certain criterion compromise. In successive design iterations one moves in the set of compromise solutions in a desired direction until no significant improvement in γ can be realized.

The primary objective in optimizing the controller parameters has been to improve regulation of the displacement error for the transition phase after switching from manual to automatic steering. Simultaneously, the displacement regulation performance should not be impaired for the other maneuvers, especially with respect to maximal guideline deviation. These specifications were translated to the design procedure using criteria of the types

$$\int_{t_1}^{t_2} y^2\, dt; \qquad \max_t |y|.$$

In addition, eigenvalue criteria were used to guarantee robust Γ-stability of the closed loop system with linear control. For sliding mode control, criteria to keep the eigenvalues of the linearized closed loop system stable, were included into the design specifications. For the linear controller design, the numerator coefficients $\boldsymbol{k} = [k_{DD}, k_D, k_P, k_I]^T$ were chosen free for optimization, whereas for the sliding mode controller the coefficients $\boldsymbol{k} = [c, \epsilon, \lambda]^T$ were chosen for optimization. The observer parameters ℓ_1, ℓ_2, M_1, and M_2 have to be determined according to measurement noise considerations as outlined in Section IV-B3. The starting values were taken from (7) for the linear controller and from Table II for the sliding mode controller. The optimization results in

$$\boldsymbol{k} = [k_{DD},\, k_D,\, k_P,\, k_I]^T = [1.108, 10.912, 24.024,\, 0.1024]^T \tag{25}$$

for the linear controller and in

$$\boldsymbol{k} = [c,\, \epsilon,\, \lambda]^T = [1.045, 0.001, 0.71]^T$$

for the sliding mode controller.

Simulations were performed for the four reference maneuvers given in the benchmark problem [1], as listed in Section II-B. For brevity only optimization results of the nonlinear controller will be shown. Fig. 13 shows the lateral displacement measured by the sensor at the front of the bus for the four maneuvers. The dashed lines mark the nonlinear controller with hand-tuned parameters, whereas the solid lines mark the optimization result. Fig. 13 displays the steering angle rate for the nonlinear controller using the approximation (24). It should be noted that in a microprocessor implementation, the adjustments derived in [8] are vital to avoid control chattering.

The figures show that the specifications given in Section II-B are met: The constraint on the steering angle rate is satisfied by the choice of M_u in (14). The limitation of the steering angle itself posed no problems in all given reference maneuvers. The lateral displacement and acceleration requirements are also fulfilled (see Fig. 13 and Fig. 14). It is difficult to determine the natural frequency of the lateral motion analytically for the nonlinear controller and, thus, it cannot be included into the optimization procedure directly. The simulations with crosswind (see the left upper graph of Fig. 13) indicates a natural frequency of the closed loop system of approximately 1.6 Hz, which is only slightly higher than given in Section II-B. The passenger comfort can be further improved by decreasing the parameters λ and c.

VI. Conclusion

Two controllers for the automatic steering problem with feedback of the lateral displacement and yaw rate have been designed, a linear one and a nonlinear sliding mode controller. In both cases a main effort was to find feasible controller structures with a few free controller parameters. These parameters were first hand-tuned and then refined by optimizing a vector performance index. The two entirely different designs (linear and nonlinear) uncover some of the inherent design conflicts that show up in both approaches. First there exists the conflict between smooth transients for passenger comfort and tight control for small lateral deviations from the guideline. The second requirement leads to faster control actions. A second design conflict is between the steering angle rate constraint and stability for the case of entering a narrow bus stop bay, where the admissible velocity should not be too low.

Both controllers meet all specifications; there are, however, some general differences in all four maneuvers. The nonlinear controller yields smaller deviations from the guideline and it has a more oscillatory behavior that shows up particularly in the lateral acceleration and in the steering angle rate, but not in the deviations from the guideline. Regarding settling times, there are no significant differences between the two controllers. In both designs the initial considerations for fixing the controller structure and finding good starting values for the controller parameters by hand-tuning was important for the success of the final optimization.

The reader, who has to solve an automatic steering problem may decide for himself if he prefers the linear or the nonlinear controller. Both of them do their task well and there is no big difference in the design effort and implementation cost. Both controllers can be improved by the use of additional sensors like lateral accelerometers at the front and rear axle. The gyro is, however, the more important sensor for the robust design and its signal is also less corrupted by noise.

References

[1] J. Ackermann and W. Darenberg, "Automatic track control of a city bus," IFAC Theory Report on Benchmark Problems for Control Systems Design, 1990.

[2] J. Ackermann and W. Sienel, "Robust control for automatic steering," in *Proc. Amer. Control Conf.*, San Diego, 1990, pp. 795–800.

[3] J. Ackermann, A. Bartlett, D. Kaesbauer, W. Sienel, and R. Steinhauser, *Robust Control: Analysis and Design of Linear Control Systems With Uncertain Physical Parameters*. London: Springer, 1993.

[4] J. Ackermann, D. Kaesbauer, and R. Münch, "Robust Γ-stability analysis in a plant parameter space," *Automatica*, vol. 27, pp. 75–85, 1991.

[5] V. I. Utkin, *Sliding Modes in Control and Optimization*. Berlin, Germany: Springer-Verlag, 1992.

[6] A. G. Bonadrev, S. A. Bondarev, N. E. Kostyleva, and V. I. Utkin, "Sliding modes in systems with asymptotic state observers," *Automation and Remote Control*, vol. 46, no. 6 (P.1), pp. 679–684, 1985.

[7] V. I. Utkin, "Application of equivalent control method to systems with large feedback gain," *IEEE Trans. Automat. Contr.*, vol. 23, pp. 484–486, 1978.

[8] J. Ackermann, J. Guldner, and V. I. Utkin, "A robust nonlinear control approach to automatic path tracking of a car," in *Proc. IEE Int. Conf. Control '94*, Coventry, UK, Mar. 1994, pp. 196–201.

[9] J. Guldner, V. I. Utkin, and J. Ackermann, "A sliding mode approach to automatic car steering," in *Proc. Amer. Control Conf.*, Baltimore, MA, 1994, pp. 1969–1973.

[10] G. Kreisselmeier and R. Steinhauser, "Systematic control design by optimizing a vector performance index," in *IFAC Symp. Computer Aided Design of Control Systems*, Zürich, 1979, pp. 113–117.

Jürgen Ackermann received the Dipl.-Ing. and Dr.-Ing. degrees from the Technical University Darmstadt, the M.S. degree from the University of California, Berkeley, and the "Habilitation" from the Technical University of Munich, Munich, Germany.

Since 1962 he has been with the German Aerospace Research Establishment (DLR), Oberpfaffenhofen, Germany, where he is currently Director of the Institute of Robotics and System Dynamics. He is also Adjunct Professor at the Technical University of Munich. His main research interests are in parametric robust control and automotive control applications. He is author of several books on "Sampled-data Control Systems" and "Robust Control."

Dr. Ackermann is a member of the IFAC Council, the European Control Conference Association and the Board of Governors of the IEEE Control Systems Society.

Jürgen Guldner received the Baccalaureate degree at the European School in Munich, Germany, and then studied at the Department of Electrical Engineering at the Technical University in Munich. In 1992 he received the M.S. degree in electrical engineering from Clemson University, Clemson, SC, where he had studied for one year as a Fulbright scholar.

Since November 1992 he has been with DLR, Germany, and is currently working on his Ph.D. thesis. His current research interests are nonlinear control theory and its application to robotic systems, and in particular motion planning, obstacle avoidance, and path control for mobile robots.

Wolfgang Sienel received the Dipl.-Ing. degree in electrical engineering in 1989 and the Dr.-Ing. degree in 1994 from the Technical University of Munich, Germany.

Since 1989 he has been a Research Assistant with the Institute of Robotics and System Dynamics at the German Aerospace Research Center (DLR). His research interests are in robust control theory, development of computer tools for analysis and design of robust control systems, and automotive control.

Reinhold Steinhauser received the Diploma degree in 1975, and in 1984, the Dr. Ing. degree from the Technical University of Karlsruhe, where he studied electrical engineering with main emphasis in control.

Since 1975 he has been working as a Research Scientist at DLR Oberpfaffenhofen, Institute of Robotics and System Dynamics. A main activity was the development of a controller design procedure based on vector performance optimization and its application to various industrial control problems. He now works with a research project on active landing gear control. His current research interests are in robust linear, and nonlinear control system design.

Vadim I. Utkin received a Dipl. in engineering from the Moscow Power Institute in 1960, a Candidate of Sciences degree (Ph.D.) in 1964 and a Doctor of Sciences degree in 1971, both from the Institute of Control Sciences in Moscow, and also an honorary Doctorate Degree from the University of Sarajevo, Yugoslavia.

In 1973, he was Head of the Discontinuous Control Systems Laboratory at the Institute of Control Sciences in Moscow, and he worked at the Polytechnical Institute in Moscow as a part-time Professor since 1977. He has held several visiting positions at the University of Illinois, USA, the University of Tokyo, Japan, the University of Genova, Italy, and is currently a Guest Scientist at the German Aerospace Research Establishment (DLR) in Oberpfaffenhofen, Germany. Currently, he is with The Ohio State University in Columbus, OH.

Dr. Utkin is author of two books on variable structure systems and sliding mode control. He served in several vice-chairman positions in the International Federation of Automatic Control (IFAC), as Chairman of the International Program Committee of the IFAC Symposia 1989 and 1991, and as an Associate Editor of the International Journal *Automatica* since 1973. He is one of the originators of the concepts of variable structure systems and sliding mode control. His current research interests are control of infinite-dimensional plants including flexible manipulators, sliding modes in discrete-time systems and their applications, and robot navigation and motion control.